Genome Medicine

RESEARCH

Open Access

The landscape of *Helicobacter pylori*-mediated DNA breaks links bacterial genotoxicity to its oncogenic potential

Hadas Sibony-Benyamini[1], Rose Jbara[1†], Tania Shubash Napso[1†], Layan Abu-Rahmoun[1†], Daniel Vizenblit[1,3], Michal Easton-Mor[1], Shira Perez[1], Alexander Brandis[2], Tamar Leshem[3], Avi Peretz[1,3] and Yaakov Maman[1*]

Abstract

Background *Helicobacter pylori* (*H. pylori*) infection is a significant risk factor for gastric cancer (GC) development. A growing body of evidence suggests a causal link between infection with *H. pylori* and increased DNA breakage in the host cells. While several mechanisms have been proposed for this damage, their relative impact on the overall bacterial genotoxicity is unknown. Moreover, the link between the formation of DNA damage following infection and the emergence of cancerous structural variants (SV) in the genome of infected cells remained unexplored.

Methods We constructed a high-resolution map of genomic *H. pylori*-induced recurrent break sites using the END-seq method on AGS human gastric cells before and after infection. We next applied END-seq to cycling and arrested cells to identify the role of DNA replication on break formation. Recurrent *H. pylori*-mediated break sites were further characterized by analyzing published RNA-seq, DRIP-seq, and GRO-seq data at these sites. γH2AX staining and comet assay were used for DNA breakage quantification. Liquid chromatography-mass spectrometry (LC–MS) assay was used to quantify cellular concentrations of dNTPs.

Results Our data indicated that sites of recurrent *H. pylori*-mediated DNA breaks are ubiquitous across cell types, localized at replication-related fragile sites, and their breakage is dependent on replication. Consistent with that, we found that *H. pylori* inflicts nucleotide depletion, and that rescuing the cellular nucleotide pool largely reduced *H. pylori*-induced DNA breaks. Intriguingly, we found that this genotoxic mechanism operates independently of *H. pylori* cag pathogenicity island (*CagPAI*) that encodes for the bacterial type 4 secretion system (T4SS), and its virulence factor, CagA, which was previously implicated in increasing DNA damage by downregulating the DNA damage response. Finally, we show that sites of recurrent *H. pylori*-mediated breaks coincide with chromosomal deletions observed in patients with intestinal-type GC and that this link potentially elucidates the persistent transcriptional alterations observed in cancer driver genes.

Conclusions Our findings indicate that dNTP depletion by *H. pylori* is a key component of its genotoxicity and suggest a link between *H. pylori* genotoxicity and its oncogenic potential.

Keywords Gastric cancer, *Helicobacter pylori*, Genome-instability, Replication stress, dNTP depletion, RRM2

†Rose Jbara, Tania Shubash Napso and Layan Abu-Rahmun share equal contributions.

*Correspondence:
Yaakov Maman
yaakov.maman@biu.ac.il
Full list of author information is available at the end of the article

Background

H. pylori is a gram-negative extracellular bacterium that colonizes the epithelial stomach and infects about half of the world's population [1]. Chronic infection with *H. pylori* causes a variety of pathologies including peptic ulceration and chronic gastritis [2, 3]. Importantly, it is the most significant risk factor of gastric cancer (GC) development [3, 4].

A growing body of evidence demonstrates that *H. pylori* infection induces the formation of double-stranded breaks (DSBs) in host cells. This genotoxic effect is primarily attributed to the bacterial cag pathogenicity island (*cag-PAI*), which encodes for the type IV secretion system (T4SS), and the secreted virulence factor CagA [5]. Indeed, studies have demonstrated the downregulation of DNA damage response (DDR) factors such as RAD51 and BRCA1 in a CagA-dependent manner [6, 7], making CagA-positive strains more genotoxic. Nevertheless, a significant portion of *H. pylori*-mediated DNA breakage retains even in the absence of CagA, arguing for a substantial CagA-independent component of *H. pylori*-genotoxicity. In this regard, *H. pylori* was recently shown to activate the ALPK1/TIFA/NF-κB pathway, which subsequently leads to the formation of RNA:DNA hybrids ("R-loops"). These structures compromise the genome integrity by promoting nuclease-mediated DNA cleavage, and replication stress [8]. This process has been demonstrated to be independent of CagA, but still relies on the presence of *CagPAI*. Of note, inhibiting NF-kB only partially reduced DSB levels, suggesting that there are additional mechanisms involved in *H. pylori* genotoxicity.

Replication stress is a major instigator of DNA damage. It arises upon stalling or slowing of the replication fork during DNA synthesis, which may occur due to dNTP depletion [9–11], or inhibition of DNA polymerase [12, 13]. Impairment of the replication fork progression results in the formation of single-stranded DNA (ssDNA) between the DNA helicase, responsible for DNA unwinding, and the lagging DNA polymerase [14]. ssDNA persistence triggers a replication-stress response that ultimately results in nuclease-mediated cleavage at the site of stalling [15, 16].

Both the CagA-dependent and CagA-independent processes described above link *H. pylori* infection to replication stress: R-loop formation may result in transcription-replication collisions (TRCs), and mis-regulation of RAD51 and BRCA1 hinders homologous-recombination (HR), thereby preventing the repair of replication-coupled DNA damage [6]. However, the contribution of replication stress to the overall *H. pylori* genotoxicity is not yet clear, as it has been reported that *H. pylori* can cause DNA damage even without DNA synthesis taking place [17].

Eradication of *H. pylori* does not revert cancer progression once initiated. This portrays a "hit-and-run" mechanism in which the infection leaves long-lived marks on cells that remain even after bacterial clearance [18]. Such persistence might be established due to DNA damage, resulting in chromosomal aberrations that can lead to oncogene hyperactivation, or the deletion of tumor-suppressor genes [19]. There is, therefore, a possibility that *H. pylori*-mediated DNA breaks are connected to the genetic landscape distinctive of GC. However, a direct link between the two is yet to be established.

In this study, we conduct a high-resolution genome-wide mapping of DSBs, to identify distinct genomic sites that recurrently undergo breakage shortly after *H. pylori* infection at the host cells. These breaks, referred to as "*H. pylori*-mediated break sites" (HPBS), appear in short genes characterized by enrichment in R-loops, as well as around repetitive DNA elements. This HPBS signature follows the pattern of the previously defined replication-coupled fragile sites [20], and coincide with break sites that appear upon hydroxyurea (HU) treatment, which induces replication stress through induction of dNTP depletion [21]. In accordance with that, we found that a large portion of *H. pylori*-induced DNA breakage is mediated by the depletion of dNTPs, which operates independently of *CagPAI*. Finally, we demonstrated that HPBS are linked to sites of chromosomal aberrations obtained in GC patients and may be a source for persistent transcriptional changes in early stages of tumorigenesis.

Methods

Antibodies

Anti-gH2A.X (S139), produced in Mouse (Abcam, Cat. No. #ab26350); Anti-RRM2, produced in Mouse (Abcam, Cat. No. # ab57653); Anti-CagA (A-10), produced in Mouse (Santa cruz, Cat. No. #sc-28368); Anti beta-Actin, produced in Rabbit (Abcam, Cat. No. # ab115777); Anti-Rabbit IgG H&L (HRP), produced in Goat (Abcam, Cat. No. # ab6721); Anti-Mouse IgG H&L (Alexa Fluor® 488), produced in Goat (Abcam, Cat. No. # ab150117); Anti-Rabbit IgG H&L (Alexa Fluor® 594), produced in Goat (Abcam, Cat. No. # ab150084).

Primers

Primers for *H. pylori* GlmM gene were used to detect *H. pylori* infection: FW (5′-CCAGGAGTGAGTGGA AGACA-3′) and RV (5′-GCAAATGAGCCTACAGCA GA-3′).

Cell culture, bacterial strains, infections, and treatments

Wild-type adenocarcinoma gastric cells (AGS) were cultured in Dulbecco's modified Eagle's medium (DMEM)

supplemented with 10% fetal bovine serum (FBS, Gibco), penicillin streptomycin, L-glutamine and sodium pyruvate (Gibco) at 37 °C. RAG1−/−preB vAbl cells—generously contributed by Dr. Andre Nussenzweig, National Cancer Institute, NIH—were cultured in RPMI supplemented with 15% FBS (Gibco), penicillin streptomycin, L-glutamine and sodium pyruvate (Gibco) at 37 °C.

The *H. pylori CagPAI*-positive (ATCC43054) and *CagPAI*-negative (ATCC51932) strains used in this work were generously provided by Clinical Microbiology Laboratory, Baruch Padeh Medical Center, Poriya, Israel. *E.coli* XL1-Blue strain was used for comparing dNTP levels and RRM2 expression (Additional File 1: Fig. S4). Infections were performed for 24 h with MOI of 100–140 (for AGS cells) and 20 (for vAbl cells). For cell cycle arrest, vAbl cells were treated with 3 mM STI-571 (Imatinib; Selleckchem #S2475) for 72 h.

Immunoblot analysis

Whole-cell lysates were prepared by suspending $2–4\times10^6$ cells in 200–400 µL of RIPA lysis buffer (1 M TrisHCl [pH 8.0], 5 M NaCl, 0.5 M EDTA, 10% IgePAL CA-630, 10% sodium deoxycholate, 10% SDS, 100 mM PMSF (0.1 M in ethanol), phosphatase inhibitors, and protease inhibitor). An equal amount of lysate protein underwent separation via 15% SDS–polyacrylamide gel electrophoresis (PAGE) and transferred to Midi-size PVDF membranes (BIO-RAD). After blocking with Blocking solution reagent (AdvanBlock Chemi; Advansta), the membranes were incubated with anti-γH2AX (1:500; Abcam), anti-Actin (1:3000), anti-RRM2 (1:200), antibodies. The membranes were washed, incubated with goat anti-rabbit IgG (1:10,000) or goat anti-mouse (1:10,000), and again washed, followed by ECL detection (Advansta). The signal was detected using the Q9 gel documentation systems. Signal intensities were normalized to Actin in all experiments.

Comet assay

Comet Assay-Kit (Abcam;ab238544) was used to conduct an Alkaline comet assay. Briefly, cells were collected and washed once in PBS, and then were combined with low-melting agarose. The cells were subsequently treated with lysis buffer and an alkaline solution, followed by electrophoresis for 30 min at 18 V under alkaline conditions. DNA staining was accomplished using Vista Green DNA Dye solution, prior to the detection of comet tails using epifluorescence microscopy Zeiss upright AxioImager M2 ApoTome through a 10× objective. Analysis of DNA in each tail was performed using ImageJ [22] (NIH) using OpenComet [23] plug-in. All images were processed with Adobe Photoshop CS5.1.

Quantification was performed using a minimum of five different fields, each containing 15–20 comets.

Immunofluorescence

Cells were seeded a concentration of 1×10^4 cells/plate in a glass bottom dish (Cellvis; Sunnyvale, CA, USA). Following treatment, the cells were rinsed with PBS and, pre-extraction was carried out with 0.1% Triton/PBS for 1 min on ice. Subsequently, the cells were fixed with 4% formaldehyde for 10 min at room temperature. Following fixation, the cells were blocked with 10% horse serum and 0.2% Tween in PBS for 1 h at room temperature. Incubation with antibodies was carried out in 1% horse serum in PBS-T using with anti-cagA antibody (1:50) and anti-γH2AX (1:1000) for 1 h at room temperature, followed by incubation with secondary, Alexa Fluor 488–goat anti-mouse IgG antibody (1:1000) or Alexa Fluor 594–goat anti-rabbit IgG antibody (1:1000) for 1 h. Images were acquired with Zeiss LSM780 inverted confocal microscope through a 63× objective.

END-seq

END-seq protocol was performed as previously described [24]. Briefly, single-cell suspensions of AGS cells (8 million), or vAbl cells (40 million for STI treated, and 20 million for cells that were not treated with STI), were washed with PBS, and resuspended in cell suspension buffer (Bio-Rad), embedded in agarose, and transferred into plug molds (Bio-Rad). Plugs were allowed to solidify at 4 °C and subsequently incubated with Proteinase K solution (Puregene, QIAGEN) for 1 h at 50 °C, followed by overnight incubation at 37 °C. This was followed by consecutive washes in a wash buffer consisting of 10 mM Tris–HCl (pH 8.0) and 50 mM EDTA (Wash Buffer) and then in a TE Buffer containing 10 mM Tris (pH 8.0) and 1 mM EDTA. Washed plugs were subsequently treated with RNaseA (Puregene, QIAGEN), washed again in Wash Buffer, and stored at 4 °C (up to 2–4 days). Blunting, A-tailing, and ligation to END-seq hairpin adaptor 1 were performed at 37 °C and 4 °C, respectively. The DNA extracted from melted plugs was fragmented to a size range of 150 and 200 bp by sonication (Covaris), followed by purification of biotinylated DNA fragments using streptavidin beads (MyOne C1, Invitrogen). After streptavidin capture, the newly generated ends underwent end repair using T4 DNA polymerase (15 U), Klenow fragment (5 U), and T4 polynucleotide kinase (15 U); A-tailed with Klenow exo-fragment (15 U), followed by ligation to END-seq hairpin adaptor 2 using the NEB Quick ligation kit. After the second adaptor ligation, libraries were prepared by first digesting the hairpins on both adapters with USER enzyme (NEB), and PCR amplified for 16 cycles using TruSeq index adapters.

PCR reactions were run on a 2% agarose gel and a smear of 200–400 bp was cut. The gel was purified using the MACHEREY–NAGEL extraction Kit (740,609.50S).

Quantification of the library was performed by KAPA Library Quantification Kit for Illumina Platforms (Roche) and using dsDNA HS Assay Kit and QUBIT (Molecular Probes, Life Technologies). Quantification was done using the Agilent HS DNA Kit and Bioanalyzer 2100. 10 nM of each library were pooled together and was diluted to 4 nM according to NextSeq manufacturer's instructions. 1.7 pM were loaded onto the flow cell with 1% PhiX library control. Libraries were sequenced by Illumina NextSeq 500 platform with single-end reads of 75 cycles according to the manufacturer's instructions.

Cell-cycle analysis

For cell-cycle analysis, cells were first fixed in 100% ethanol, after which they underwent RNase treatment (1 mg/ml; Invitrogen) and staining with 50 µg/ml Propidium iodide (Sigma #P4170). The cell-cycle was analyzed using The Gallios Flow Cytometer.

LC–MS dNTPs quantification

AGS cells (1×10^6 cells) were collected with or without *H. pylori* infection, washed with PBS, and then snap-frozen pellet was made for each treatment. Intracellular dNTPs concentration was determined via Alexander Brandis at Life Sciences Core Facilities, Weizmann Institute of Science, 7,670,001 Rehovot, Israel.

Samples were extracted with 600 µl of chilled methanol and 400 µl of 10 mM ammonium acetate and 5 mM ammonium bicarbonate, pH 7.7. 13C10-adenosine 5′-triphosphate (13C10-ATP, Sigma) was added to standards and samples as internal standard (100 µM). After shaking at ambient temperature for 10 min (1000 rpm, Thermomixer C, Eppendorf), the samples were centrifuged (20,000 g, 5 min). Supernatants were collected and evaporated in speedvac and lyophilizer. The residues were re-suspended in 50 µl of 50%-aqueous acetonitrile, filtered, and analyzed by LC–MS/MS.

Quantification of nucleotides was carried out using an Acquity I-class UPLC system coupled to Xevo TQ-S triple quadrupole mass spectrometer (both Waters). The UPLC was performed using an Atlantis Premier BEH Z-HILIC column 2.1×150 mm 1.7 µm (Waters). The mobile phase A consisted of 17% acetonitrile in 20 mM ammonium carbonate at pH 9.25, while mobile phase B comprised acetonitrile. The flow rate was kept at 300 µl/ml consisting of a 0.8-min hold at 80% B, followed by a linear gradient decrease of B to 20% B during 4.8 min. The column temperature was set at 25 °C and an injection volume of 5 µl. An electrospray ionization interface was used as ionization source. Analysis was performed in positive ionization mode. Analytics were detected using multiple-reaction monitoring, using argon as the collision gas: 468 > 112.2 and 192.1 m/z (collision energy 12 eV for both) for dCTP, 483 > 207.2 and 81.0 m/z (collision energy 6 and 12 eV respectively) for dTTP, 492.1 > 136.2 and 81.1 m/z (collision energy 16 and 24 eV respectively) for dATP, 507.9 > 152.1 m/z (collision energy 30 eV) for dGTP, and 519.1 > 141.1 m/z (collision energy 35 eV) for 13C10-ATP. Quantification was made using a standard curve in the 0–10 µM concentration range. TargetLynx (Waters) was used for data analysis.

Immunohistochemistry (IHC) staining

Biopsy specimens (see the "Cohort description" section below) were stained for RRM2 using the BenchMark ULTRA IHC semi-automatic device (Ventana Co., Tucson, AZ, USA) with the assistance of the pathology laboratory at the Tzafon Medical Center, Poria, Israel. Briefly, the Formalin-Fixed Paraffin-Embedded (FFPE)biopsy specimens are sliced into 4-µm-thick sections. The specimens are deparaffinized in EZprep (Ventana Co.), at 72 °C, followed by antigen retrieval at 95 °C, for 64 min, in buffer CC1 (Roche, Indianapolis, IN, USA). Slides were preheated for 4 min, at 36 °C, and then incubated with a primary antibody (mouse 1:200, abcam, Cambridge, UK) for 20 min and detected with Ventana UltraView Universal DAB Buffer (Roche). The slides were stained with hematoxylin, washed, and dehydrated in increasing ethanol concentrations. Images are captured using an EVOS™ Imaging System (Invitrogen). Analysis was done on ImageJ using Color Deconvolution plugin [25, 26].

Cohort description

Gastric biopsy specimens collected from 11 different patients with median age of 63, who underwent esophagogastroduodenoscopy (EGD) at the Tzafon Medical Center between 2022 and 2024 and classified as *H. pylori* positive ($n=5$) or negative ($n=6$) by pathological examination.

Statistical analysis

Statistical analyses throughout the study were performed using R version 4.1.2 (http://www.r-project.org). The statistical tests are reported in the figure legend and main text. In comparisons where *T*-test was applied, the Shapiro–Wilk test was used to determine data normality for compared variables.

Fisher's exact test was used to compare the distribution of genomic sites overlapping with HPBS to expected distribution using comparable randomely-picked regions (see the "Genome annotation" section below).

Support vector machine classification was used to predict breakabilty of genes and TA-repeats following infection, using the e1071 package in R [27].

Genome alignment

END-seq reads were aligned to either the human (hg19) genome, or the mouse (GRCm38p2/mm10) genome, using *Bowtie* (version 1.1.2) [28] with the options: –best–all –strata –l 50. For END-seq – we allowed 3 mismatches and kept the best strata for tags with multiple alignments (-n 3 –k 1). For ChIP-seq, we allowed 2 mismatches and discarded reads with multiple alignments (-n 2 –m 1). For GRO-seq, 3 mismatches were allowed (–n 3 –m1). *Samtools* was used to convert the sam output file to bam file [29].

Peak calling

To identify *H. pylori*-mediated END-seq peaks (with or without DRB treatment), *H. pylori*-infected replicates were combined and *MACS* 1.4.3 [30] was used for peak calling with default parameters (*p*-value cutoff for peak detection of $1\times10E-5$;–keep-dup = auto), using the combined uninfected data as control. Data from uninfected cells served as control, with peaks retained if exhibiting > tenfold-enrichment. Next, the reads-per-kb-per-million-reads (RPKM) was calculated for each of the *H. pylori*-infected samples using *bedtools intersect* [31] function. Only peaks that exhibited at least twofold increase in each *H. pylori*-infected sample over the combined uninfected sample, were retained.

Differential breakage analysis

Differential breakage analysis was conducted as follows: Total END-seq read counts across gene bodies (from TSS to TTS; see the "Genome annotation" section below), or TA repeats (+/−250 bp from the repeat center) was calculated for each dataset of *H. pylori*-infected and uninfected sampels, and served as an input for DESeq2 [32] package (release 1.30.1) in R (version 4.1.2). Cutoffs of Fold-change and adjusted *p*-values are indicated in the corresponding figure legends.

Genome annotation

Transcription start sites (TSSs) and gene body coordinated were defined using RefSeq [33] genes annotations (genome build hg19/GRCh37.p13 for human, and mm10 for mouse), taken from the UCSC database [34]. Repetitive elements were obtained from RepeatMasker [35].

R package "*LOLA*" [36] was used to test the enrichment of diffferent genomic regions within *H. pylori*-mediated break sites. Annotations of enhancers and LADs were obtained from the internal *LOLA* database.

Random genomic sites used for comparison with HPBS, where obtained by applying *bedtools shuffle*[31] function on HPBS, while excluding sites overlapping with HPBS and retaining the relative distribution among chromosomes.

Data visualization

For genome browser tracks visualization, aligned bed files were converted into bedgraph using *bedtools genomecov* [31], followed by bedGraphToBigWig [37] to make a bigwig file. Values were normalized to reads per million. Genomic profiles were visualized using the Integrative Genomic Viewer (IGV) browser [38]. For aggregate plots, the signal was smoothed using *smooth.spline* function in R. Volcano plots of differential breakage analysis were generated using the "*EnhancedVolcano*" package [39] (release 1.8.0) in R.

Results

High-resolution mapping of *H. pylori*-induced breakome

To gain a comprehensive view of *H. pylori*-mediated DNA breakage, AGS gastric cells were infected with *H. pylori* (ATCC 43504;*CagPAI*-positive strain) for 24 h (Additional file 1: Fig. S1A). *H. pylori*-mediated DNA breaks were detected by immunostaining for the repair factor γH2AX and by comet assay (Additional file 1: Fig. S1B,C).

Next, *H. pylori* infected cells were subjected to END-seq for genome-wide mapping of DSBs (see the "Methods" section) [24, 40, 41]. Overall, ~1700 recurrent break sites, hereinafter termed "*H. pylori*-induced break sites" ("HPBS"), were identified across the genome (Fig. 1A). In general, HPBS presented a signature of active chromatin, showing enrichment predominantly at gene bodies and promoters (Fig. 1B; top; (Additional file 1: Fig. S1D). Among the intergenic regions, HPBS sites were localized at gene-rich regions (Fig. 1B) and were characterized by enrichment in repetitive DNA elements (Additional file 1: Fig. S1D).

Closer examination revealed two classes of HPBS, distinguished by their localization and structure: the first class consisted of genic sites that span the entire gene body and extended to its flanking regions (Fig. 1C; left), while HPBS from the second class were mainly situated within intergenic regions and were highly focal (Fig. 1C; right).

To explore the properties of genes harboring DSBs, we conducted a comparison of breakage levels across all genes in cells infected with *H. pylori* and those in uninfected cells. The analysis revealed 419 genes that have significantly higher levels of DSBs in the infected cells ("HPBS genes"; Fig. 1D; left panel; Additional file 2: Table S1). Analysis of published RNA-seq from AGS cells

[42, 43], showed that HPBS genes are highly transcribed and exceptionally short in comparison to unbroken genes (Fig. 1D; right panel).

Support vector machine classification (Additional file 1: Fig. S1E) showed that HPBS genes can be effectively predicted based on their transcription level and size.

We next examined the intergenic HPBS. The signal in this class of break sites, presented two sharp peaks from opposite strands. As mentioned, these sites were highly enriched at repetitive DNA sequences (Fig. 1E; Additional file 1: Fig. S1D), with TA-repeats being significantly enriched at break sites over randomly selected genomic sites.

Of note, out of ~66 k TA-repeats, 197 repeat acquired DSBs to significantly high levels following infection (Additional file 1: Fig. S1F).

Previous reports attributed the fragility of tandem repeats to their size and purity [44, 45]. In agreement with that, TA repeats that undergo breakage following *H. pylori* infection were characterized by large size and high purity (Additional file 1: Fig. S1G).

Moreover, support vector machine (SVM) classification using repeat size and purity as predictors demonstrated that TA-repeat breakability after infection can be effectively predicted, achieving an area under the curve (AUC) of 0.85 (Additional file 1: Fig. S1H,I).

Taken together, *H. pylori* infection induces recurrent DNA breakage at hundreds of genomic sites, that can be divided into two classes: highly transcribed, short genes, and TA-repeats.

Breakage at HPBS is associated with DNA replication

Previous studies linked *H. pylori*-mediated damage to replication stress [6, 8, 46], while others demonstrated replication-independent DNA damage following infection [17]. Given that both repetitive DNA elements [47–49] and transcribed regions [47–49] were recognized as hotspots of replication fork stalling and DNA breakage in replication stress conditions, we next sought to explore the involvement of replication in the formation of the HPBS described above.

To enable sufficient timeframe for infection following cell-cycle arrest, without inducing replication stress, we used the mouse pre-B cell line, vAbl, which can be efficiently arrested in G1 phase for up to 72 h through treatment with the kinase inhibitor STI-571 [50] (Fig. 2A; Additional file 1: Fig. S2A). To examine the effect of cell cycle arrest on DNA breakage, we treated cells with STI-571 for 48 h. Following that, once cells were largely arrested (Additional file 1: Fig. S2A), we infected them with *H. pylori* for 24 h. These arrested cells were compared to *H. pylori*-infected cells that were not treated with STI-571 ("Dividing cells") (Fig. 2B).

Dividing vAbl cells presented a breakage pattern similar to the pattern observed in the AGS gastric cells, featuring enrichment at genic sites and gene-rich regions (Additional file 1: Fig. S2B,C).

Similar to genic HPBS from AGS data, vAbl genic HPBS showed a preference for short and highly transcribed genes (Fig. 2B, C, D, Additional file 1: Fig. S2D).

Notably, genic HPBS from the two cell lines exhibited minimal overlap (Additional file 1: Fig. S2E). These differences likely stem from the transcriptomic disparities between the two cell lines, as vAbl genic HPBS that do not overlap with AGS genes are transcribed at significantly lower levels in AGS cells (Additional file 1: Fig. S2F).

Overall, our data shows that HPBS genes are ubiquitous across cell types, and that vAbl cells provide a suitable platform for our investigation.

Strikingly, upon cell cycle arrest, genic HPBS were diminished (Fig. 2E, F, Additional file 1: Fig. S2G). Thus, DNA replication is necessary for breakage to occur at HPBS.

(See figure on next page.)

Fig. 1 The landscape of *H. pylori*-mediated breakage. **A** END-seq profiles of data from *H. pylori* infected (two upper panels; red) and uninfected (two lower panels; blue) AGS cells are shown. Values are given in reads-per-million. **B** Top: The 1673 *H. pylori*-mediated break sites (HPBS), determined by peak calling (see the "Methods" section), were categorized based on their genomic localization into intergenic regions, gene bodies, and promoters (left pie chart). The same number of randomly picked sites (right pie chart) were used for comparison (Fisher's test; $p < 1E-10$). Bottom: Histogram showing the distances from the closest genes for intergenic HPBS (red) and randomly selected regions (gray). (*T*-test; $p < 1E10$). Three biological replicates from infected and uninfected cells were used. **C** Zoom-in of END-seq profiles of genic (left) and intergenic (right) HPBS. **D** Left: Volcano plot showing differential breakage analysis (see the "Methods" section) across all genes between END-seq data from *H. pylori*-infected and uninfected AGS cells. Genes exhibiting significantly elevated END-seq signal in infected cells (referred to as HPBS genes; defined by -log10(adjusted *p*-value) > 2 and abs(Log2FC) > 1) are highlighted in red ($N = 419$). Right: histograms showing the differences in the distribution of transcription levels (top) and gene size (bottom) between HPBS genes (red) and unbroken genes (blue). (Wilcoxon rank-sum test; $p < 1E-10$, for both comparisons). Three biological replicates from infected and uninfected cells were used. **E** Top: Zoom-in on intergenic break site exhibiting two distinct peaks indicative of two DNA ends separated by a gap with (TA)n repeat sequence. Bottom: Enrichment analysis of repetitve DNA elements wthin intergenic HPBS and randomly picked regions (see the "Methods" section). Fisher's exact test with FDR of $*q < 0.05$; $***q < 1e-10$. **F** Cumulative plot of the relative END-seq signal at 20-kb window around TSS and transcription termination sites (TES) of HPBS genes. Values (HP/UI) represent the ratio between signal from *H. pylori*-infected and uninfected cells

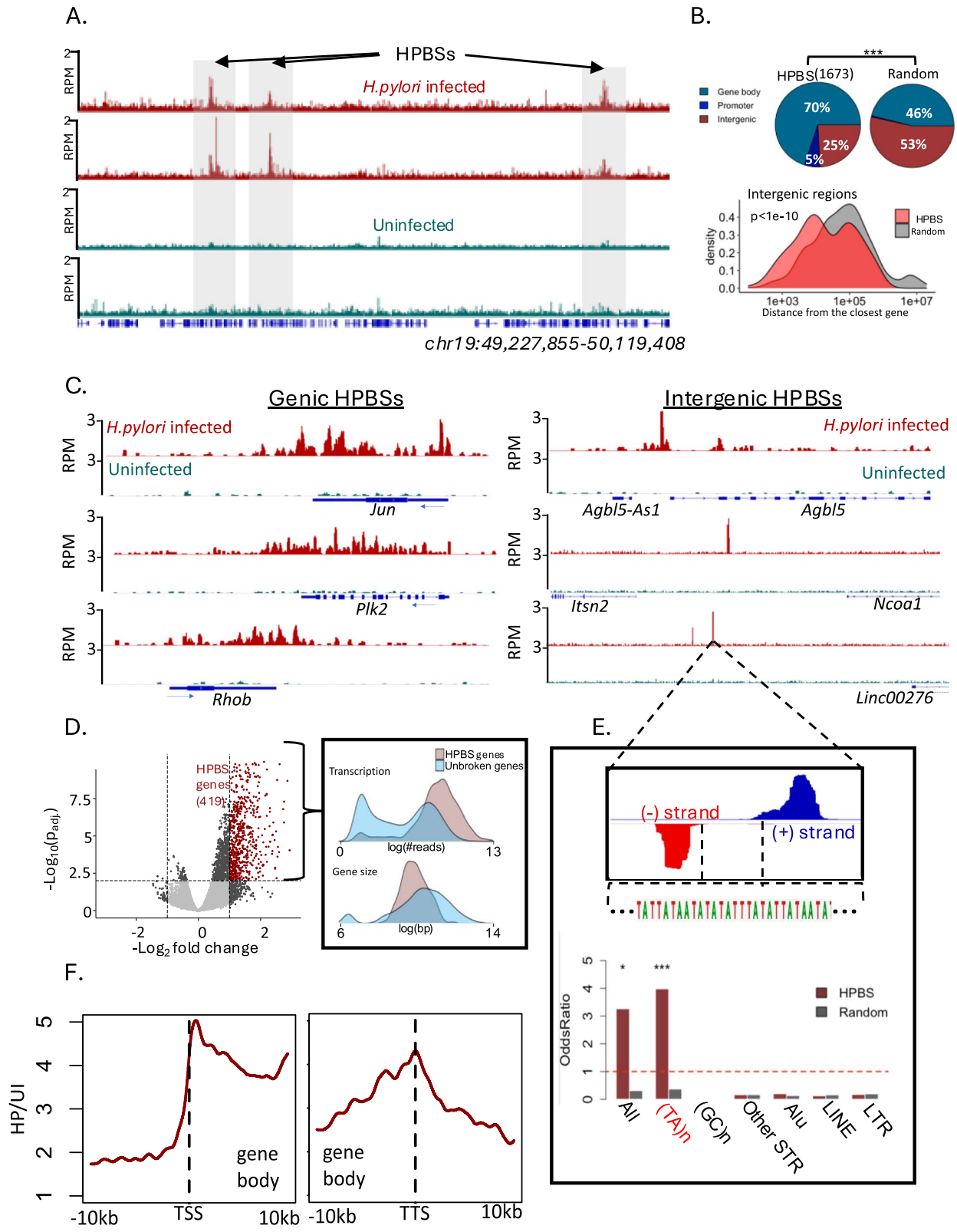

Fig. 1 (See legend on previous page.)

Replication fork stalling at genes may occur by transcription-replication collision (TRC) [51, 52], and the formation of R-loops [53–55]. We therefore hypothesized that HPBS genes are prone to R-loop formation. To test this idea, we compared the vAbl breakage pattern to R-loop patterns obtained by published DRIP-seq data performed on mouse B cells [56, 57].

Consistent with the replication-coupled characteristics of the DSBs sites, the DRIP-seq analysis revealed that HPBS genes are indeed characterized by high levels of R-loops (Fig. 2G, H). Importantly, while R-loop formation correlates with levels of transcription, HPBS genes exhibited higher levels of R-loops, and shorter length compared to other highly transcribed genes (GRO-seq [58, 59]; Fig. 2H). This finding consistent with a previous study demonstrating that short genes are prone to R-loops formation [60]. To further strengthen the link between DSBs and R-loop formation, we divided the genes into 5 quantiles with respect to their breakage levels, and obtained the level of R-loops across the genes from the different quantiles. The differential signal of R-loops between the quantiles indicates that DSB levels in HPBS genes are predictive of their R-loop levels (Fig. 2I, Additional file 1: Fig. S2H). Taken together, our data indicates that breaks in HPBS are formed during replication, and that genic HPBS are notably enriched in R-loops.

dNTP depletion is a key source for *H. pylori*-mediated DNA damage

One of the major causes of replication stress is the shortage of dNTPs. Of note, DSB profiles of cells that undergo dNTP depletion by treatment with hydroxyurea (HU), inhibitor of the ribonucleotide reductase (RNR) subunit RRM2, showed a breakage profile reminiscence of the breakage signature observed *H. pylori* infected cells, characterized by a notable enrichment of DSB at gene-rich regions and repetitive DNA elements [48]. We therefore wondered whether DNA breaks induced by *H. pylori* are initiated by dNTP depletion.

To test this, we first measured the cellular dNTP concentration in *H. pylori*-infected and uninfected AGS cells by liquid chromatography-mass spectrometry (LC–MS) assay (see the "Methods" section). Strikingly, *H. pylori*-infected cells showed a substantial decrease in dNTP levels (Fig. 3A; Additional file 1: Fig. S3A). Consistently, we identified *H. pylori*-induced downregulation of RRM2 expression, in both transcript and protein levels (Fig. 3B and C, respectively). Similar RRM2 decrease has been observed by Immunohistochemical staining of gastric mucosa biopsies obtained from *H. pylori*-infected and uninfected individuals (Additional file 1: Fig. S3D) for RRM2 (Fig. 3D).

Since RRM2 expression is normally upregulated in S-phase [61], one could argue that the decreased levels of RRM2 in *H. pylori*-infected cells simply reflects cell cycle arrest in response to *H. pylori* infection. However, cell cycle analysis showed that infected cells progress to S-phase as frequently as uninfected cells (Additional file 1: Fig. S3B). Thus, it can be concluded that *H. pylori*-mediated RRM2 downregulation is not merely a consequence of overall cell cycle arrest.

To assess the extent by which *H. pylori* genotoxicity is driven by dNTP depletion, we supplemented the infected cells with an external reservoir of dNTPs that partially recovered their dNTP pool (Fig. 3A and Additional file 1: Fig. S3A; light red bars). Strikingly, the recovery of dNTP levels significantly decreased DNA break levels in infected cells, reaching levels comparable to those observed in uninfected cells (Fig. 3C and Additional file 1: Fig. S3C).

(See figure on next page.)

Fig. 2 Genic *H. pylori*-mediated break sites are replication-coupled. **A** Schematic representation of the experimental setup for infecting arrested cells: cells were treated STI-571 for 72 h. Following 48 h of STI treatment, cells were infected with *H. pylori* for 24 h (see the "Methods" section). **B** Genomic profile of END-seq from *H. pylori*-infected (red) and uninfected (green) dividing (– STI) and arrested (+ STI) vAbl cells. **C** Zoom-in on genic breaks from END-seq profiles of dividing vAbl cells infected with *H. pylori* (red), or uninfected (green). **D** Volcano plot showing differential breakage analysis (see the "Methods" section) across all genes between END-seq data from *H. pylori*-infected and uninfected dividing vAbl cells (adjusted *p*-value < 0.05; abs(Log2FC > 1)). Genes exhibiting significantly higher END-seq signals in infected cells (HPBS genes) are highlighted in red. Two biological replicates for each condition were used. **E** Zoom-in on genic breaks from END-seq profiles of arrested vAbl cells infected with *H. pylori* (red), or uninfected (green). **F** Volcano plot presenting differential breakage analysis (see the "Methods" section) across all genes between END-seq data from *H. pylori*-infected and uninfected vAbl cells, following cell cycle arrest by STI treatment. (adjusted *p*-value < 0.05; abs(Log2FC > 1). Two biological replicates for each condition were used. **G** Genomic profiles of END-seq from *H. pylori*-infected (red) and uninfected (green) dividing vAbl cells, along with GRO-seq (black; from *Bönelt P, 2019*) and DRIP-seq (blue; from *L.,Chédin,2022*) data. Two representative HPBS genes (left) and two highly transcribed, unbroken genes (right), are displayed. **H** Boxplots showing the quantification of transcription (by GRO-seq), and DSBs (by END-seq), gene size, and R-loop levels (by DRIP-seq) in broken genes (red) from data of dividing vAbl cells. For comparison, unbroken genes with comparable levels of transcription (gray) were picked (framed plots; two-tailed *T*-test; *ns-p* > 0.05 for transcription, and ***$p < 1e-10$ for DSBs). The two sets were then compared for their gene size and R-loops levels. *T*-test; **$p < 1E-6$ and *$p < 0.004$, respectively. **I** A DRIP-seq signal is presented for five gene sets, grouped by quantiles of DSB levels in cycling vAbl cells, as measured by END-seq, in infected cells

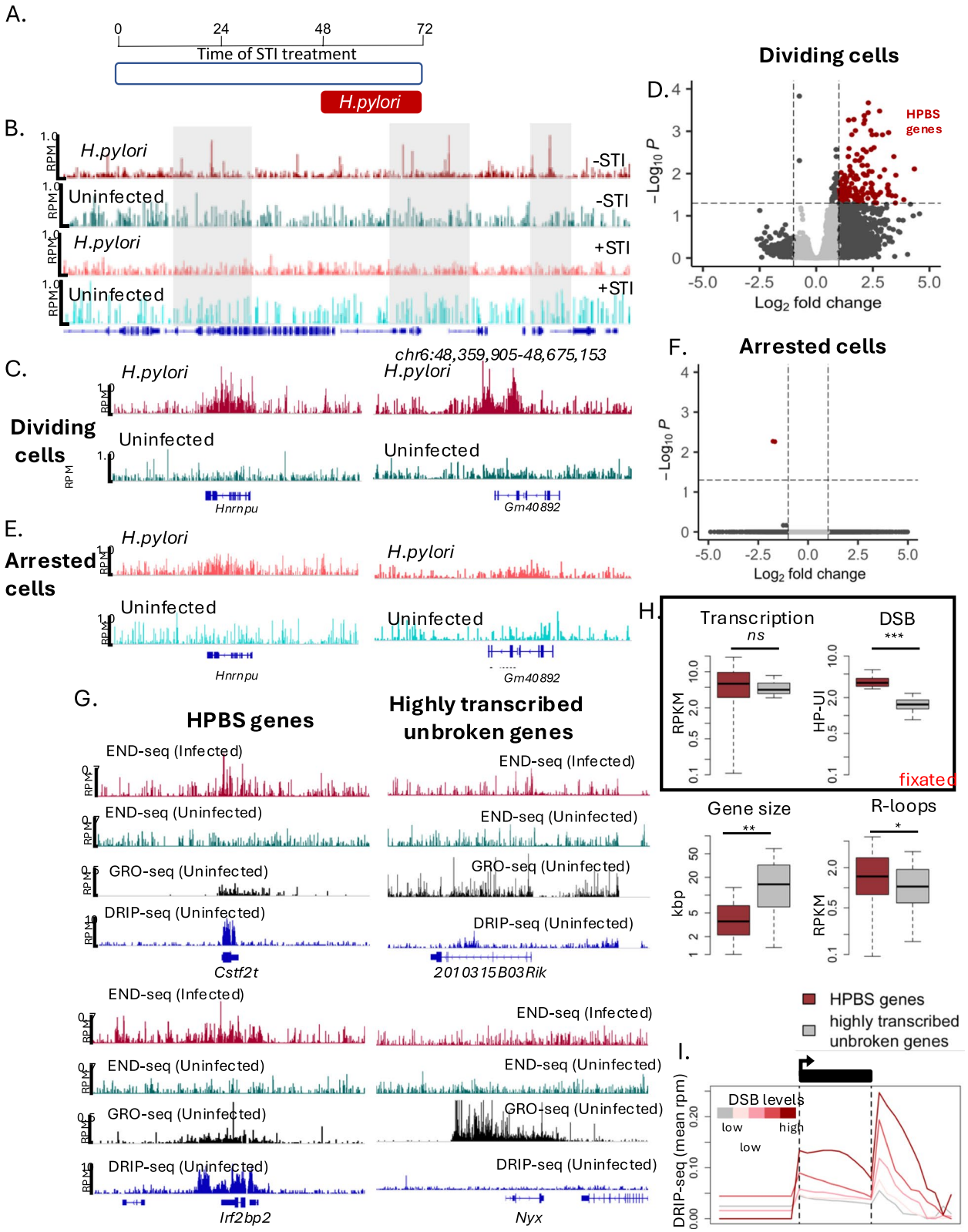

Fig. 2 (See legend on previous page.)

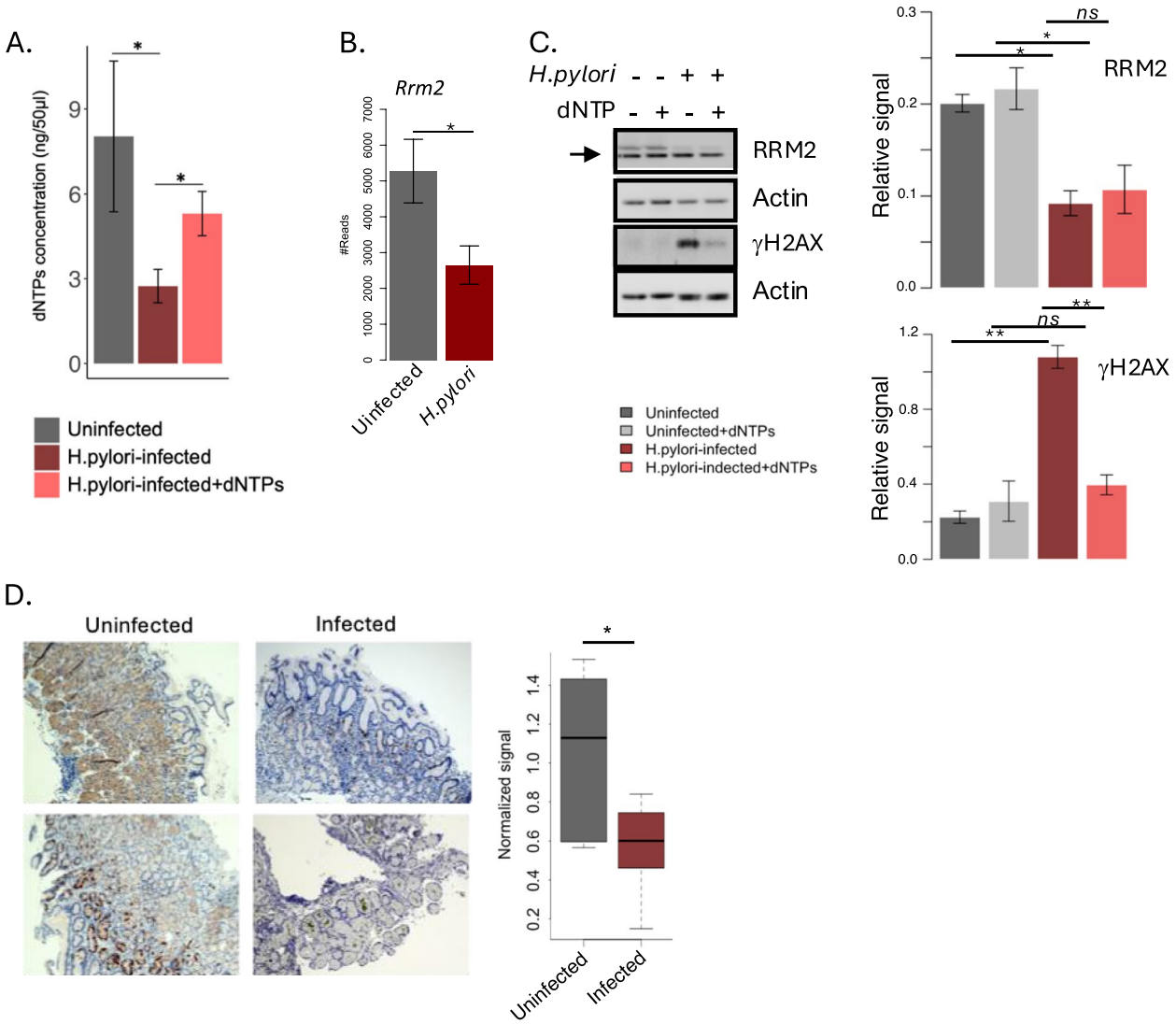

Fig. 3 dNTP depletion is a key source for *H. pylori*-mediated DNA damage. **A** Cellular concentration of dNTPs was measured by LC–MS (see the "Methods" section) for uninfected (gray) and *H. pylori*-infected cells (dark red), supplemented with 50 µM of dNTPs. (*T*-test; $p < 0.05$ for both comparisons). At least 3 biological replicates from each condition were used. **B** Number of RNA-seq reads (from Kontizas et al.) of Rrm2 gene in samples from uninfected (gray) and *H. pylori*-infected cells (red). (*Wald test; adjusted *p*-value < 0.05). **C** Left: Immunoblotting for RRM2 (top) γH2AX (middle) and Actin (bottom) in uninfected and infected AGS cells, with and without external supplementation of dNTPs. Right: Immunoblotting quantification for RRM2 and γH2AX ($n = 3$ per group). *$p < 0.05$. **D** Left: Biopsy specimens from individuals positive and negative to *H. pylori* were stained for RRM2 (brown) and hematoxylin (blue). Right: RRM2 signal, normalized with hematoxylin stain following color deconvolution (see the "Methods" section). Five *H. pylori*-positive samples and 6 *H. pylori*-negative samples were used in the analysis. The values were obtained by averaging all images per individual (**T*-test; $p < 0.05$)

***H. pylori*-mediated dNTP depletion is independent of CagA**

According to previous reports, *H. pylori* can induce DNA breakage by both CagA-dependent and CagA-independent mechanisms.

Thus, we wondered whether dNTP depletion by *H. pylori*, and the resulting DNA damage are dependent on the presence of CagA. To address this inquiry, we compared cells infected with *CagPAI*-positive ("*CagA*(+)";ATCC 43504) and *CagPAI*-negative ("*CagA*(−)";ATCC51932) *H. pylori* strains. Consistent with previous reports [5, 8], both *CagA*(+) and *CagA*(−) strains show increased levels of DNA damage compared to uninfected cells, while the extent of DNA breakage in cells infected with *CagA*(−) strain was significantly lower than that observed in the *CagA*(+) infected cells (Fig. 4A). In contrast, the levels of dNTP depletion, as well as the downregulation of RRM2, were comparable between the two strains (Fig. 4B). This observation is

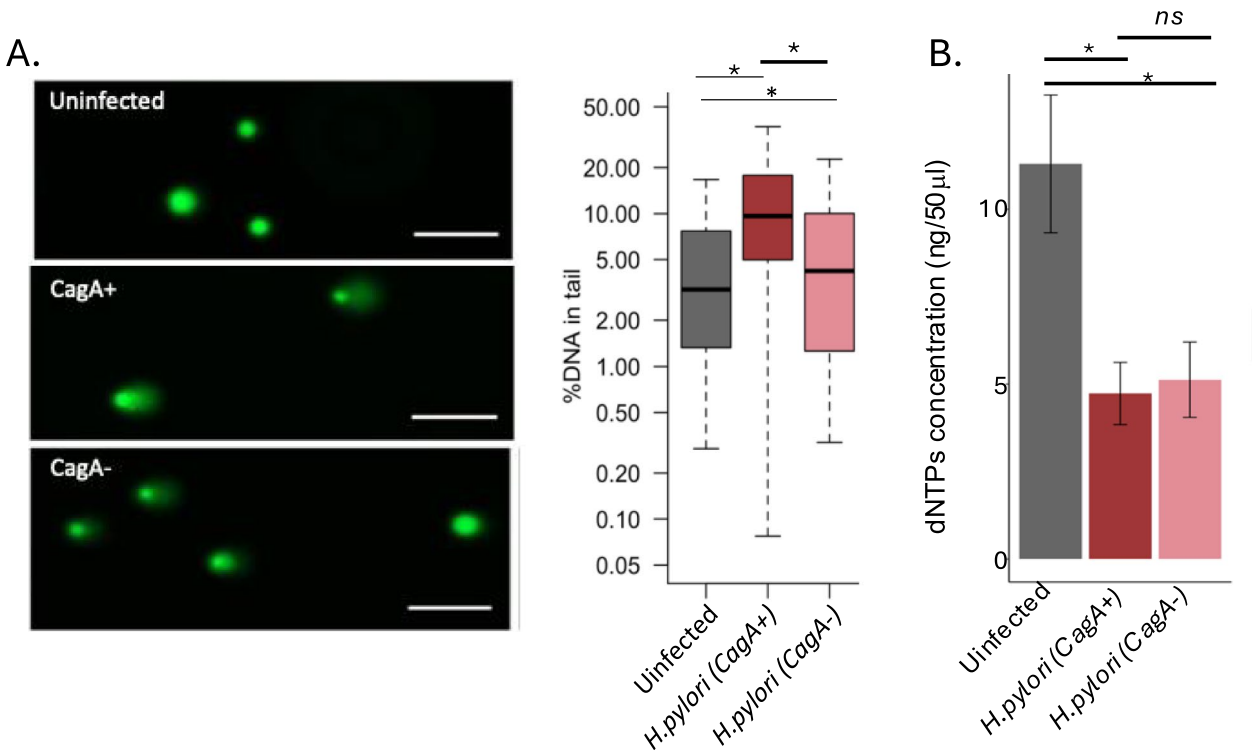

Fig. 4 dNTP depletion by *H. pylori* is independent of CagA. **A** Left: Visualization of stained DNA from uninfected cells (gray) and cells infected with CagA + (dark red) and CagA – (pink) *H. pylori* strains, subjected to comet assay. Right: quantification of percentage of the DNA in the tail from the total DNA for each cell. Wilcoxon rank-sum test; $p < 1E-3$. At least 5 replicates were used for each condition. The presented values were obtain by averaging the signal from all cells for each replicate. **B** Cellular concentration of dNTPs was quantified using LC–MS (see the "Methods" section) for uninfected (gray), *H. pylori*-(CagA +)-infected cells (dark red) and *H. pylori*-(CagA –)-infected cells (pink) (*T*-test; $*p < 0.01$)

consistent with the downregulation of Rrm2 transcript observed in P12 *H. pylori* strain as well as its isogenic DCagA mutant (Additional file 1: Fig. S3E). Of note, infection with laboratory *E.coli* strain did not result in dNTP depletion (Additional file 1: Fig. S3F), suggesting that dNTP depletion—albeit independent of CagA—is a characteristic feature of *H. pylori* infection.

DNA breakage caused by *H. pylori* is manifested in GC chromosomal aberrations

H. pylori infection increases the risk of developing GC. However, the contribution of its genotoxic impact to this risk remains unknown.

To explore this possible link, we inquired whether the DNA breakage caused by *H. pylori* is evident in genetic variants of patients with gastric cancer (GC). GC is traditionally divided into two types: intestinal-type and diffuse-type. It is well accepted that chronic *H. pylori* infection is associated with intestinal-type GC, whereas the connection between *H. pylori* and diffuse-type GC remained uncertain [62, 63].

Thus, we analyzed structural variants from 100 GC patients [64]. Fifty-seven of these patients were diagnosed with intestinal-type GC and therefore were hypothesized to exhibit discernible signatures indicative of HPBS. The remaining 43 patients were diagnosed with GC from a diffused/mixed type. Additionally, genetic data of non-gastric cancers, acute lymphoblastic leukemia, prostate cancer, and skin cancer [65], were used as negative controls.

Using the data sets above, we quantified the cumulative breakage signal within a 500-kb window centered on the deletion breakpoints. Strikingly, END-seq signals from the infected cells presented significant enrichment of breakage signal near breakpoints from intestinal-type GC data, but not from any of the other data sets (Fig. 5A, B). Hence, deletions of intestinal-type GC patients display HPBS signature.

Previous studies showed that *H. pylori* infection leads to differential expression (DE) of multiple genes, including cancer-related genes [42, 66]. We reasoned that these DE genes can be categorized into two distinct classes: the first class involves DE resulting from the reversible perturbation of cellular process by the bacteria, whereas the second class occurs due to long-lived chromosomal changes. Importantly, the latter can persist even after

bacterial clearance and may play a role in cancer transformation. We hypothesize that *H. pylori*-mediated breakage facilitates these persistent alternation.

To test this hypothesis, we analyzed a set of previously identified GC driver genes [64]. This set consists of 97 cancer-related genes that recurrently undergo deletion/amplification. Based on our END-seq data, increased breakage was detected in 13 of these genes following *H. pylori* infection (Fig. 5C, E). We tested the correlation between the infection-driven differential expression ("infection DE"), and the transcriptional changes observed between tumor and normal tissue ("cancer DE"). Strikingly, a significant correlation between infection DE and cancer DE was observed for the 13 genes broken upon *H. pylori* infection, though not for the unbroken genes (Fig. 5D), suggesting that *H. pylori*-mediated breakage initiates GC tumorigenesis by prompting copy-number variations and transcriptional changes at GC driver genes. Together, these results point towards a causal link between the genotoxic effect of *H. pylori* and the tumorigeneses of GC.

Discussion

The capacity of *H. pylori* to induce DNA breakage in host cells is now widely accepted. Here, we utilized high-resolution mapping of DNA double-strand breaks (DSB) to illustrate the "breakome" induced by *H. pylori*, identifying two distinct classes of breaks: intergenic breaks, enriched at TA repeats, and genic breaks, enriched at short, highly transcribed genes, where breakage levels correlate with R-loop levels.

Of note, Koeppel et al. [67] have been previously conducted γH2AX ChIP-seq on *H. pylori*-infected and uninfected cells. Consistent with our data, their study revealed γH2AX enrichment following infection at transcribed regions. In comparison to γH2AX ChIP-seq, where signal resolution is limited both due to the technical aspects of ChIP-seq and the nature of γH2AX signal spreading outwards the break sites, the high sensitivity and resolution of END-seq allowed us to identify specific break sites in a precise and quantitative fashion, such that the mechanisms of breakage can be inferred.

Interestingly, beyond highly transcribed genes, Koeppel et al. identified infection-derived γH2AX peaks at pre-telomeric regions that were not identified by our data. The differences between the two profiles may reflect a discrepancy between the sites of double-strand breaks (DSBs) and γH2AX formation, potentially resulting from the natural distribution bias of unphosphorylated H2AX across the genome. In line with this, Seo et al. [68] demonstrated that non-phosphorylated H2AX is enriched in sub-telomeric region, supporting an inherent bias in γH2AX accumulation towards sub-telomeric breaks. Whether this bias could also account for the absence of γH2AX signal at repetitive DNA elements, which showed high signal in our data, requires further investigation.

The breakage pattern that emerged from our map points toward replication-coupled DNA damage. Further investigation in this direction portrayed a model (Fig. 5F) wherein *H. pylori* infection induces dNTP depletion and replication stress, independently of CagA, by downregulating RRM2. Consequent to replication stress, a distinct pattern of breakage is formed at previously annotated replication barriers, including repetitive elements and bodies of short genes that are prone to R-loop formation. These sites—which we collectively named HPBS—are reflected in oncogenic chromosomal deletions observed in GC and correlate with transcriptional perturbation of GC driver genes. This provides a potential mechanism

(See figure on next page.)

Fig. 5 *H. pylori*-mediated breakage is manifested in chromosomal deletions from GC patients. **A** END-seq profiles depict normalized intensities of DSBs data from H. pylori-infected AGS cells (upper panel; red) contrasted with uninfected AGS cells (lower panel; blue). Horizontal bars represent deleted regions obtained from patients with intestinal-type GC (Wang et al. 2014). Dashed lines represent the breakpoints of these deletions. **B** Plots showing cumulative END-seq signal of *H. pylori* infected (red) and uninfected AGS cells (blue) within 500 kb window centered around breakpoints. Data is organized from left to right for patients with intestinal GC, diffused/mixed type GC (Wang et al. 2014; with breakpoint numbers 7053 and 2765, respectively), acute lymphoblastic leukemia, prostate cancer, and skin cancer ($n = 2389$, 4235, and 10,915, respectively; all sourced from COSMIC) (*T*-test; $p < 1E-4$ for intestinal GC data, and $p > 0.05$ for the other data sets). **C** Volcano plot showing differential breakage analysis (see the "Methods" section) across GC driver genes (from Wang 2014) between END-seq data from *H. pylori*-infected and uninfected dividing vAbl cells (adjusted *p*-value < 0.05; abs(Log2FC > 1)). Driver genes with significantly higher END-seq signal at infected cells ($N = 13$) are shown in red. **D** Scatter plots showing the correlation between log2(fold-change) in the expression between tumor and normal tissue (*x*-axis; data from Wang 2014), and between infected and uninfected AGS cells (*y*-axis; data from Kontizas 2020), for broken GC driver genes (left; $r = 0.65$; $p < 0.02$) and unbroken GC driver genes (right). Pearson correlation test; $r = 0.65$; $p < 0.02$ for broken genes, and $r = 0.05$; $p = 0.62$, for unbroken genes. **E** Genomic profiles of END-seq from *H. pylori*-infected (red) and uninfected (green) AGS cells. Two representative broken GC driver genes are presented. **F** Proposed model: *H. pylori* infection facilitates genome instability by a combination of CagA-independent and CagA-dependent mechanisms: CagA-independent genotoxicity is primarily based on the downregulation of *Rrm2*, dNTP depletion, and, finally, the formation of replication-coupled DNA breakage at bodies of genes with a tendency to produce R-loops, and at repetitive DNA elements. CagA suppresses the DNA damage response, thereby promoting the propagation of DNA breaks into long-lived chromosomal aberrations

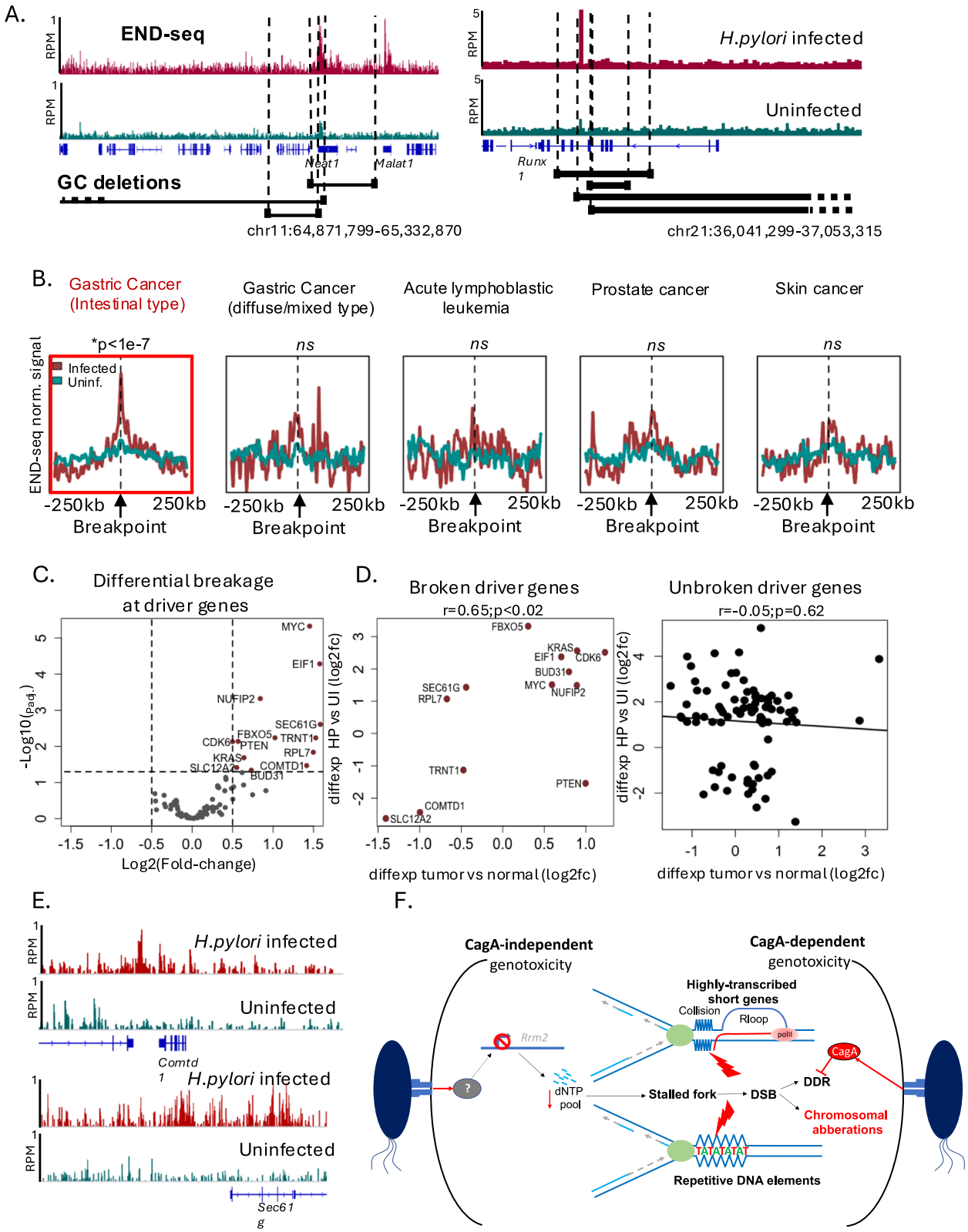

Fig. 5 (See legend on previous page.)

through which *H. pylori* infection contributes to GC development.

Our findings demonstrate that supplementing external dNTPs is sufficient in reducing γH2AX signal to background levels (Fig. 3C). This observation underscores the significance of the CagA-independent depletion of dNTPs in the genotoxic effects of *H. pylori*. On the other hand, consistent with previous reports, our data shows that cells infected with CagA(+) strain present increased DNA damage (Fig. 4A). This excessive genotoxicity observed in CagA(+) strains is likely linked to its ability to impede DNA damage response [6, 7].

As mentioned earlier, Bauer et al. proposed a mechanism of *H. pylori* genotoxicity in which bacterial ADP-heptose is secreted into host cells, triggering ALPK1/TIFA/NF-κB signaling activation and resulting in R-loop accumulation. While this is a notable example of a CagA-independent mechanism, it still relies on CagPAI, which encodes the bacterial T4SS responsible for secreting ADP-heptose. In contrast, the mechanism proposed here—initiated by dNTP depletion—takes place in the absence of *CagPAI*.

The identity of the host and bacterial factors that link *H. pylori* infection to dNTP depletion is yet to be revealed. Of note, the transcriptional program active during the S-phase, which includes the upregulation of RRM2 [69], is initiated by the transcription factor E2F1. E2F1 is regulated by its interaction with Retinoblastoma (Rb). This interaction brings Rb to the promoters of E2F1 target genes where it suppresses their transcription by recruiting transcription repressors [70]. Normally, upon G1/S transition, Rb undergoes phosphorylation and is released from E2F1, allowing the latter to activate the transcription of its targets [71]. A possible mechanism is, therefore, that the downregulation of RRM2 following infection is caused by perturbation of Rb/E2F1 pathway.

From the bacterial side, an intriguing hypothesis is associated with *H. pylori*'s ability to activate the Toll-like receptor 2 (TLR2) through interaction with UreB, a subunit of the bacterial urease enzyme [72, 73]. This interaction has been demonstrated to induce the expression of the hypoxia-induced factor 1a (HIF1a), which canonically mediates the cell response to hypoxia [73]. The upregulation of HIF1a may, in turn, contribute to dNTP depletion through several mechanisms: Firstly, HIF1a has been shown to inhibit the E2F1-mediated transcriptional program by upregulating the expression of E2F7 and interacting with it at the promoters of E2F1-responsive genes [74]. In addition, during hypoxia, RRM2—which is oxygen-sensitive—loses its activity, and later its expression, being replaced by RRM2B, an isoform less sensitive to oxygen. While this substitution partially rescues the dNTP pool and increase replication efficiency, it does not restore them to normal levels [75]. Therefore, HIF1α represents an intriguing target for future studies investigating *H. pylori* genotoxicity.

Under normal conditions, a depletion of dNTPs and the subsequence replication stress would lead to cell cycle arrest [76, 77]. However, our observation revealed that infected cells continue to cycle as frequently as uninfected cells, suggesting that the transmission of the DNA damage response to cell cycle regulation is somehow hindered. Such decoupling might be attributed to the previously documented CagA-dependent downregulation of p53 [78–80], which blocks the induction of cell cycle arrest in response to replication stress. Additionally, our data suggests a connection between *H. pylori*-mediated damage and the formation of long-lived chromosomal aberrations, including copy number variations in GC driver gene. Thus, allowing cell cycle progression alongside extensive DNA breakage can lead to transcriptional changes that further promote dysregulated cell proliferation and survival.

Collectively, a comprehensive two-tier model can be outlined for *H. pylori* genotoxicity and its role in gastric cancer tumorigenesis. In this model (Fig. 5F), *H. pylori* actively induces DNA damage in host cells, through dNTP depletion independently of CagA. Simultaneously, CagA contributes to the attenuation of repair processes for this damage, while maintaining cell cycle progression by downregulating p53.

Of note, pathogen-induced dNTP depletion has been demonstrated before in Human Papillomavirus (HPV) infection [9]. However, while *H. pylori*-induced dNTP depletion has been shown here to be decoupled from cell cycle progression, HPV-induced dNTP depletion occurs in the context of cell cycle dysregulation, and premature entry into S-phase with insufficient dNTP concentration. Despite this difference, the common genotoxic pathway shared by these two oncogenic pathogens may suggest a more universal characteristic of pathogen-related tumorigenesis.

Although mostly related to gastric epithelial tissue pathologies, *H. pylori* infection is not restricted to gastric cells. Previously, systematic analysis of *H. pylori* infection and cell responses in multiple non-gastric human and mouse cell lines [81], revealed a wide range of cell types that can be efficiently infected with *H. pylori*, and demonstrated an array of *H. pylori*-induced cellular responses. Moreover, *H. pylori* has been shown to induce DNA damage in U2OS human osteosarcoma cells [17]. Consistent with these observations, we show here that *H. pylori* infects and induces DSBs in mouse pre-B cells (vAbl). Importantly, we demonstrate that the genotoxic effect of *H. pylori* on those cells is reminiscent of its effect on human gastric cells (AGS), both in its relation

to replication and in the DSB pattern. Notably, *H. pylori* infection has been linked to the development of MALT lymphoma, a B-cell neoplasia of the digestive tract. The similarity that we observed here between gastric and lymphoid cells in *H. pylori*-mediated DSB signature, implies some commonalities in the etiology of these two *H. pylori*-mediated cancers.

While our data argues that *H. pylori*-mediated breaks may be a source for CNVs shown in GC driver genes, this genotoxicity-oncogenicity axis is yet to be established. Of note, 89% of non-cardia GC cases are attributable to *H. pylori* [82]. However, considering the high frequency of *H. pylori* in the total population, there is likely a significantly lower fraction of GC cases where *H. pylori* played a major role in tumorigenesis. Nevertheless, for this subset, the extended time window of several decades between infection and cancer transformation offers a unique opportunity to early detect the initiation of cancerous processes through *H. pylori*-mediated breaks leading to persistent chromosomal aberrations that can be monitored over time.

Conclusions

We provide a novel model of *H. pylori* genotoxicity, in which *H. pylori* induces dNTP depletion in host cells through a CagA-independent mechanism, leading to replication-coupled DNA breaks. Furthermore, we show that *H. pylori* infection imposes a signature of recurrent DNA break sites, which are reflected in chromosomal aberrations in GC patients, suggesting a link between *H. pylori* genotoxicity, and the genetic etiology of GC.

Supplementary Information

The online version contains supplementary material available at https://doi.org/10.1186/s13073-025-01439-3.

Additional file 1: Includes Supplementary Figures S1-S3.

Additional file 2: Includes Table S1.

Acknowledgements

The authors express their gratitude to Dr. Andres Canela for his invaluable assistance in establishing the END-seq experiments. Additionally, they would like to thank both Dr. Andres Canela and Dr. Sriram Sridharan for their valuable advice, Dr. Marina Kurtz for her support in genomic library assembly, Dr. Yehuda Gubbay for his assistance with the cell-cycle analyses, and Mr. Tevie Mehlman for his assistance with dNTP quantification.

Authors' contributions

HSB, RJ, TSN, LAR, DV, and AB performed the experiments; YM, HSB, and MEM wrote the manuscript; SP generated the genomic libraries; YM and HSB performed the data analysis; TL established the bacterial growth and infection; YM and AP supervised the study. All authors read and approved the final manuscript.

Funding

This study was partially supported by the Israeli Science Foundation (ISF;1920/20 to YM), Israel Cancer Association (ICA; 20220096 to YM), Israel Cancer Research Fund (ICRF; 23–201-RCDA to YM), and The Goldberg Foundation (246043 to YM).

Data availability

The accession number for the END-seq data reported in this paper is NCBI GEO: GSE245644. The accession numbers of the public genomic data used in the study are as follows: RNA-seq: GSE162056 [43]; DRIP-seq: GSE201210 [57]; GRO-seq: GSE111692 [59].

Declarations

Ethics approval and consent to participate

Research involved human samples (immunohistochemistry) was approved by Helsinki Committee of the Baruch Padeh Medical Center, Poriya, (Approval no. POR 0007–20).

Competing interests

The authors declare that they have no competing interests.

Author details

[1]Azrieli Faculty of Medicine in the Galilee, Bar-Ilan University, Zefat, Israel. [2]Life Sciences Core Facilities, Weizmann Institute, Rehovot, Israel. [3]Baruch Padeh Medical Center, Poriya, Israel.

Received: 18 April 2024 Accepted: 13 February 2025
Published: 24 February 2025

References

1. Chmiela M and Kupcinskas J. Review: Pathogenesis of Helicobacter pylori infection. Helicobacter. 2019;24. https://doi.org/10.1111/hel.12638.
2. Correa P and Piazuelo MB. The gastric precancerous cascade. J Dig Dis. 2012;13. https://doi.org/10.1111/j.1751-2980.2011.00550.x.
3. Watari J, Chen N, Amenta PS, Fukui H, Oshima T, Tomita T, Miwa H, Lim KJ, and Das KM. Helicobacter pylori associated chronic gastritis, clinical syndromes, precancerous lesions, and pathogenesis of gastric cancer development. Preprint. 2014. https://doi.org/10.3748/wjg.v20.i18.5461 https://doi.org/10.3748/wjg.v20.i18.5461.
4. Díaz P, Valderrama MV, Bravo J and Quest AFG. Helicobacter pylori and gastric cancer: Adaptive cellular mechanisms involved in disease progression. Preprint. 2018. https://doi.org/10.3389/fmicb.2018.00005 https://doi.org/10.3389/fmicb.2018.00005.
5. Murata-Kamiya N, Hatakeyama M. Helicobacter pylori-induced DNA double-stranded break in the development of gastric cancer. Cancer Sci. 2022;113:1909–18. https://doi.org/10.1111/cas.15357.
6. Imai S, Ooki T, Murata-Kamiya N, Komura D, Tahmina K, Wu W, Takahashi-Kanemitsu A, Knight CT, Kunita A, Suzuki N, et al. Helicobacter pylori CagA elicits BRCAness to induce genome instability that may underlie bacterial gastric carcinogenesis. Cell Host Microbe. 2021;29. https://doi.org/10.1016/j.chom.2021.04.006.
7. Han T, Jing X, Bao J, Zhao L, Zhang A, Miao R, Guo H, Zhou B, Zhang S, Sun J, et al. H. pylori infection alters repair of DNA double-strand breaks via SNHG17. J Clin Investig. 2020;130:3901–39018. https://doi.org/10.1172/JCI125581.
8. Bauer M, Nascakova Z, Mihai AI, Cheng PF, Levesque MP, Lampart S, Hurwitz R, Pfannkuch L, Dobrovolna J, Jacobs M, et al. The ALPK1/TIFA/NF-κB axis links a bacterial carcinogen to R-loop-induced replication stress. Nat Commun. 2020;11. https://doi.org/10.1038/s41467-020-18857-z.
9. Bester AC, Roniger M, Oren YS, Im MM, Sarni D, Chaoat M, Bensimon A, Zamir G, Shewach DS and Kerem B. Nucleotide deficiency promotes genomic instability in early stages of cancer development. Cell. 2011;145. https://doi.org/10.1016/j.cell.2011.03.044.
10. Saldivar JC, Miuma S, Bene J, Hosseini SA, Shibata H, Sun J, Wheeler LJ, Mathews CK and Huebner K. Initiation of Genome Instability and Preneoplastic Processes through Loss of Fhit Expression. PLoS Genet. 2012;8. https://doi.org/10.1371/journal.pgen.1003077.
11. Burrell RA, McClelland SE, Endesfelder D, Groth P, Weller MC, Shaikh N, Domingo E, Kanu N, Dewhurst SM, Gronroos E, et al. Replication

stress links structural and numerical cancer chromosomal instability. Nature. 2013;494. https://doi.org/10.1038/nature11935.
12. Glover TW, Berger C, Coyle J and Echo B. DNA polymerase α inhibition by aphidicolin induces gaps and breaks at common fragile sites in human chromosomes. Hum Genet. 1984;67. https://doi.org/10.1007/BF00272988.
13. Durkin SG and Glover TW. Chromosome fragile sites. Preprint. 2007. https://doi.org/10.1146/annurev.genet.41.042007.165900.
14. Tanaka T and Nasmyth K. Association of RPA with chromosomal replication origins requires an Mcm protein, and is regulated by Rad53, and cyclin- and Dbf4-dependent kinases. EMBO Journal. 1998;17. https://doi.org/10.1093/emboj/17.17.5182.
15. Nam EA and Cortez D. ATR signaling: more than meeting at the fork Edward. Biochem J. 2013;436. https://doi.org/10.1042/BJ20102162.ATR.
16. Maréchal A and Zou L. DNA damage sensing by the ATM and ATR kinases. Cold Spring Harb Perspect Biol. 2013;5. https://doi.org/10.1101/cshperspect.a012716.
17. Toller IM, Neelsen KJ, Steger M, Hartung ML, Hottiger MO, Stucki M, Kalali B, Gerhard M, Sartori AA, Lopes M, et al. Carcinogenic bacterial pathogen Helicobacter pylori triggers DNA double-strand breaks and a DNA damage response in its host cells. Proc Natl Acad Sci U S A. 2011;108. https://doi.org/10.1073/pnas.1100959108.
18. Hatakeyama M. Helicobacter pylori CagA and gastric cancer: A paradigm for hit-and-run carcinogenesis. Preprint. 2014. https://doi.org/10.1016/j.chom.2014.02.008.
19. Kou F, Wu L, Ren X and Yang L. Chromosome Abnormalities: New Insights into Their Clinical Significance in Cancer. Preprint. 2020. https://doi.org/10.1016/j.omto.2020.05.010.
20. Barlow J, Faryabi RB, Callen E, Wong N, Malhowski A, Chen HT, Gutierez-Cruz G, Sun HW, Mckinnon P, Wright G, et al. A novel class of early replicating fragile sites that contribute to genome instability in B cell lymphomas. Cell. 2013;152(3):620–32.
21. Koç A, Wheeler LJ, Mathews CK and Merrill GF. Hydroxyurea Arrests DNA Replication by a Mechanism that Preserves Basal dNTP Pools. J Biol Chem. 2004;279. https://doi.org/10.1074/jbc.M303952200.
22. Abràmoff MD, Magalhães PJ and Ram SJ. Image processing with imageJ. Preprint. 2004. https://doi.org/10.1201/9781420005615.ax4 https://doi.org/10.1201/9781420005615.ax4.
23. Gyori BM, Venkatachalam G, Thiagarajan PS, Hsu D, and Clement MV. OpenComet: An automated tool for comet assay image analysis. Redox Biol. 2014;2. https://doi.org/10.1016/j.redox.2013.12.020.
24. Canela A, Maman Y, Jung S, Wong N, Callen E, Day A, Kieffer-Kwon KR, Pekowska A, Zhang H, Rao SSP, et al. Genome Organization Drives Chromosome Fragility. Cell. 2017;507–521. https://doi.org/10.1016/j.cell.2017.06.034.
25. Schindelin J, Arganda-Carreras I, Frise E, Kaynig V, Longair M, Pietzsch T, Preibisch S, Rueden C, Saalfeld S, Schmid B, et al. Fiji: An open-source platform for biological-image analysis. Preprint. 2012. https://doi.org/10.1038/nmeth.2019 https://doi.org/10.1038/nmeth.2019.
26. Ruifrok AC, Johnston DA. Quantification of histochemical staining by color deconvolution. Anal Quant Cytol Histol. 2001;23(4):291–9.
27. Meyer D, Dimitriadou E, Hornik K, Weingessel A, Leisch F. e1071: Misc Functions of the Department of Statistics, Probability Theory Group (Formerly: E1071), TU Wien. R package version 1.7-16; 2024. https://www.CRAN.R-project.org/package=e1071.
28. Langmead B, Trapnell C, Pop M and Salzberg SL. Ultrafast and memory-efficient alignment of short DNA sequences to the human genome. Genome Biol. 2009;10. https://doi.org/10.1186/gb-2009-10-3-r25.
29. Li H, Handsaker B, Wysoker A, Fennell T, Ruan J, Homer N, Marth G, Abecasis G and Durbin R. The Sequence Alignment/Map format and SAMtools. Bioinformatics. 2009;25. https://doi.org/10.1093/bioinformatics/btp352.
30. Zhang Y, Liu T, Meyer CA, Eeckhoute J, Johnson DS, Bernstein BE, Nussbaum C, Myers RM, Brown M, Li W, et al. Model-based analysis of ChIP-Seq (MACS). Genome Biol.2008;9. https://doi.org/10.1186/gb-2008-9-9-r137.
31. Quinlan AR and Hall IM. BEDTools: A flexible suite of utilities for comparing genomic features. Bioinformatics. 2010;26. https://doi.org/10.1093/bioinformatics/btq033.
32. Love MI, Huber W and Anders S. Moderated estimation of fold change and dispersion for RNA-seq data with DESeq2. Genome Biol. 2014;15. https://doi.org/10.1186/s13059-014-0550-8.
33. O'Leary NA, Wright MW, Brister JR, Ciufo S, Haddad D, McVeigh R, Rajput B, Robbertse B, Smith-White B, Ako-Adjei D, et al. Reference sequence (RefSeq) database at NCBI: Current status, taxonomic expansion, and functional annotation. Nucleic Acids Res. 2016;44. https://doi.org/10.1093/nar/gkv1189.
34. Karolchik D, Hinricks AS, Furey TS, Roskin KM, Sugnet CW, Haussler D and Kent WJ. The UCSC table browser data retrieval tool. Nucleic Acids Res. 2004;32. https://doi.org/10.1093/nar/gkh103.
35. Smit A, Hubley R, Green P. RepeatMasker Open-4.0; 2013. Available from: https://www.repeatmasker.org.
36. Sheffield NC and Bock C. LOLA: Enrichment analysis for genomic region sets and regulatory elements in R and Bioconductor. Bioinformatics. 2016;32. https://doi.org/10.1093/bioinformatics/btv612.
37. Kent WJ, Zweig AS, Barber G, Hinrichs AS and Karolchik D. BigWig and BigBed: Enabling browsing of large distributed datasets. Bioinformatics. 2010;26. https://doi.org/10.1093/bioinformatics/btq351.
38. Thorvaldsdóttir, H., Robinson, J.T., and Mesirov, J.P. (2013). Integrative Genomics Viewer (IGV): High-performance genomics data visualization and exploration. Brief Bioinform *14*. https://doi.org/10.1093/bib/bbs017.
39. Blighe K, Rana S and Lewis M. EnhancedVolcano: Publication-ready volcano plots with enhanced colouring and labelin. Preprint. 2019.
40. Wong N, John S, Nussenzweig A, Canela A. END-seq: An Unbiased, High-Resolution, and Genome-Wide Approach to Map DNA Double-Strand Breaks and Resection in Human Cells. In Methods in Molecular Biology. 2021. https://doi.org/10.1007/978-1-0716-0644-5_2.
41. Sciascia N, Nussenzweig A, Canela A, Sridharan S, Tubbs A, Sleckman BP, Meltzer P. DNA Breaks and End Resection Measured Genome-wide by End Sequencing. Mol Cell. 2016;63:898–911. https://doi.org/10.1016/j.molcel.2016.06.034.
42. Kontizas E, Tastsoglou S, Karamitros T, Karayiannis Y, Kollia P, Hatzigeorgiou AG and Sgouras DN. Impact of helicobacter pylori infection and its major virulence factor caga on dna damage repair. Microorganisms. 2020;8. https://doi.org/10.3390/microorganisms8122007.
43. Kontizas E, Tastsoglou S, Karamitros T, Karayiannis Y, Kollia P, Hatzigeorgiou AG, and Sgouras DN. Expression of genes related to H. pylori infection and its virulence factor CagA, in AGS cells. Gene Expression Omnibus (GEO). 2020. https://www.ncbi.nlm.nih.gov/geo/query/acc.cgi?acc=GSE162056.
44. Gemayel R, Cho J, Boeynaems S and Verstrepen KJ. Beyond junk-variable tandem repeats as facilitators of rapid evolution of regulatory and coding sequences. Preprint. 2012. https://doi.org/10.3390/genes3030461 https://doi.org/10.3390/genes3030461.
45. Legendre M, Pochet N, Pak T and Verstrepen KJ. Sequence-based estimation of minisatellite and microsatellite repeat variability. Genome Res. 2007;17. https://doi.org/10.1101/gr.6554007.
46. He J, Nascakova Z, Leary P, Papa G, Valenta T, Basler K and Müller A. Inactivation of the tumor suppressor gene Apc synergizes with H. pylori to induce DNA damage in murine gastric stem and progenitor cells. Sci Adv. 2023;9. https://doi.org/10.1126/sciadv.adh0322.
47. van Wietmarschen N, Sridharan S, Nathan WJ, Tubbs A, Chan EM, Callen E, Wu W, Belinky F, Tripathi V, Wong N, et al. Repeat expansions confer WRN dependence in microsatellite-unstable cancers. Nature. 2020;586. https://doi.org/10.1038/s41586-020-2769-8.
48. Tubbs A, Sridharan S, van Wietmarschen N, Maman Y, Callen E, Stanlie A, Wu W, Wu X, Day A, Wong N, et al. Dual Roles of Poly(dA:dT) Tracts in Replication Initiation and Fork Collapse. Cell. 2018;174. https://doi.org/10.1016/j.cell.2018.07.011.
49. McMurray CT. Mechanisms of trinucleotide repeat instability during human development. Preprint. 2010. https://doi.org/10.1038/nrg2828 https://doi.org/10.1038/nrg2828.
50. Muljo SA and Schlissel MS. A small molecule Abl kinase inhibitor induces differentiation of Abelson virus-transformed pre-B cell lines. Preprint. 2003. https://doi.org/10.1038/ni870 https://doi.org/10.1038/ni870.
51. Bermejo R, Capra T, Jossen R, Colosio A, Frattini C, Carotenuto W, Cocito A, Doksani Y, Klein H, Gómez-González B, et al. The replication checkpoint protects fork stability by releasing transcribed genes from nuclear pores. Cell. 2011;146. https://doi.org/10.1016/j.cell.2011.06.033.
52. Tuduri S, Crabbé L, Conti C, Tourrière H, Holtgreve-Grez H, Jauch A, Pantesco V, de Vos J, Thomas A, Theillet C, et al. Topoisomerase I suppresses genomic instability by preventing interference between

replication and transcription. Nat Cell Biol. 2009;11. https://doi.org/10.1038/ncb1984.
53. Bermejo R, Lai MS and Foiani M. Preventing Replication Stress to Maintain Genome Stability: Resolving Conflicts between Replication and Transcription. Preprint. 2012. https://doi.org/10.1016/j.molcel.2012.03.001.
54. Helmrich A, Ballarino M, Nudler E and Tora L. Transcription-replication encounters, consequences and genomic instability. Preprint. 2013. https://doi.org/10.1038/nsmb.2543.
55. Aguilera A and García-Muse T. R Loops: From Transcription Byproducts to Threats to Genome Stability. Preprint. 2012. https://doi.org/10.1016/j.molcel.2012.04.009.
56. Zhao H, Hartono SR, de Vera KMF, Yu Z, Satchi K, Zhao T, Sciammas R, Sanz L, Chédin F and Barlow J. Senataxin and RNase H2 act redundantly to suppress genome instability during class switch recombination. Elife. 2022;11. https://doi.org/10.7554/ELIFE.78917.
57. Zhao H, Hartono S, De Vera K, Yu Z, Satchi K, Zhao T, Sciammas R, Sanz L, Chedin F and Barlow J. Senataxin and RNase H2 act redundantly to suppress genome instability during class switch recombination. Gene Expression Omnibus (GEO). 2022. https://www.ncbi.nlm.nih.gov/geo/query/acc.cgi.
58. Bönelt P, Wöhner M, Minnich M, Tagoh H, Fischer M, Jaritz M, Kavirayani A, Garimella M, Karlsson MC and Busslinger M. Precocious expression of Blimp1 in B cells causes autoimmune disease with increased self-reactive plasma cells. EMBO J. 2019;38. https://doi.org/10.15252/embj.201810010.
59. Bönelt P, Minnich M, Woehner M, Tagoh H, Fischer M, Jaritz M, Karlsson MC, Ebert A, and Busslinger M. Precocious expression of Blimp1 in the B cell lineage causes autoimmunity. Gene Expression Omnibus. 2018. https://www.ncbi.nlm.nih.gov/geo/query/acc.cgi?acc=GSE111692.
60. Chen YH, Keegan S, Kahli M, Tonzi P, Fenyö D, Huang TT and Smith DJ. Transcription shapes DNA replication initiation and termination in human cells. Nat Struct Mol Biol. 2019;26. https://doi.org/10.1038/s41594-018-0171-0.
61. Grolmusz VK, Karászi K, Micsik T, Tóth EA, Mészáros K, Karvaly G, Barna G, Szabó PM, Baghy K, Matkó J, et al. Cell cycle dependent RRM2 may serve as proliferation marker and pharmaceutical target in adrenocortical cancer. Am J Cancer Res. 2016;6(9):2041–53.
62. Zhang XY, Zhang PY and Aboul-Soud MAM. From inflammation to gastric cancer: Role of Helicobacter pylori. Preprint. 2017. https://doi.org/10.3892/ol.2016.5506.
63. Peek RM and Blaser MJ. Helicobacter pylori and gastrointestinal tract adenocarcinomas. Preprint. 2002. https://doi.org/10.1038/nrc703 https://doi.org/10.1038/nrc703.
64. Wang K, Yuen ST, Xu J, Lee SP, Yan HHN, Shi ST, Siu HC, Deng S, Chu KM, Law S, et al. Whole-genome sequencing and comprehensive molecular profiling identify new driver mutations in gastric cancer. Nat Genet. 2014;46. https://doi.org/10.1038/ng.2983.
65. Tate JG, Bamford S, Jubb HC, Sondka Z, Beare DM, Bindal N, Boutselakis H, Cole CG, Creatore C, Dawson E, et al. COSMIC: The Catalogue Of Somatic Mutations In Cancer. Nucleic Acids Res. 2019;47. https://doi.org/10.1093/nar/gky1015.
66. Li N, Ouyang Y, Chen S, Peng C, He C, Hong J, Yang X, Zhu Y and Lu NH. Integrative Analysis of Differential lncRNA/mRNA Expression Profiling in Helicobacter pylori Infection-Associated Gastric Carcinogenesis. Front Microbiol. 2020;11. https://doi.org/10.3389/fmicb.2020.00880.
67. Koeppel M, Garcia-Alcalde F, Glowinski F, Schlaermann P and Meyer TF. Helicobacter pylori Infection Causes Characteristic DNA Damage Patterns in Human Cells. Cell Rep.2015;11. https://doi.org/10.1016/j.celrep.2015.05.030.
68. Seo J, Kim SC, Lee HS, Kim JK, Shon HJ, Salleh NLM, Desai KV, Lee JH, Kang ES, Kim JS, et al. Genome-wide profiles of H2AX and γ-H2AX differentiate endogenous and exogenous DNA damage hotspots in human cells. Nucleic Acids Res. 2012;40. https://doi.org/10.1093/nar/gks287.
69. Fouad S, Hauton D and D'Angiolella V. E2F1: Cause and Consequence of DNA Replication Stress. Preprint. 2021.https://doi.org/10.3389/fmolb.2020.599332.
70. Lees JA, Saito M, Vidal M, Valentine M, Look T, Harlow E, Dyson N and Helin K. The Retinoblastoma Protein Binds to a Family of E2F Transcription Factors. Mol Cell Biol. 1993;13. https://doi.org/10.1128/mcb.13.12.7813-7825.1993.
71. Araki K, Nakajima Y, Eto K and Ikeda MA. Distinct recruitment of E2F family members to specific E2F-binding sites mediates activation and repression of the E2F1 promoter. Oncogene. 2003;22. https://doi.org/10.1038/sj.onc.1206840.
72. Koch KN, Hartung ML, Urban S, Kyburz A, Bahlmann AS, Lind J, Backert S, Taube C and Müller A. Helicobacter urease-induced activation of the TLR2/NLRP3/IL-18 axis protects against asthma. J Clin Invest. 2015;*125*. https://doi.org/10.1172/JCI79337.
73. Valenzuela-Valderrama M, Cerda-Opazo P, Backert S, González MF, Carrasco-Véliz N, Jorquera-Cordero C, Wehinger S, Canales J, Bravo D and Quest AFG. The Helicobacter pylori urease virulence factor is required for the induction of hypoxia-induced factor-1α in gastric cells. Cancers (Basel). 2019;11. https://doi.org/10.3390/cancers11060799.
74. De Bruin A, Cornelissen PWA, Kirchmaier BC, Mokry M, Iich E, Nirmala E, Liang KH, Vegh AMD, Scholman KT, Groot Koerkamp MJ, et al. Genome-wide analysis reveals NRP1 as a direct HIF1α-E2F7 target in the regulation of motorneuron guidance in vivo. Nucleic Acids Res. 2015;44. https://doi.org/10.1093/nar/gkv1471.
75. Foskolou IP, Jorgensen C, Leszczynska KB, Olcina MM, Tarhonskaya H, Haisma B, D'Angiolella V, Myers WK, Domene C, Flashman E, et al. Ribonucleotide Reductase Requires Subunit Switching in Hypoxia to Maintain DNA Replication. Mol Cell. 2017;66. https://doi.org/10.1016/j.molcel.2017.03.005.
76. Ho CC, Siu WY, Lau A, Chan WM, Arooz T and Poon RYC. Stalled replication induces p53 accumulation through distinct mechanisms from DNA damage checkpoint pathways. Cancer Res. 2006;66. https://doi.org/10.1158/0008-5472.CAN-05-1790.
77. Pelletier J, Riaño-Canalias F, Almacellas E, Mauvezin C, Samino S, Feu S, Menoyo S, Domostegui A, Garcia-Cajide M, Salazar R, et al. Nucleotide depletion reveals the impaired ribosome biogenesis checkpoint as a barrier against DNA damage . EMBO J. 2020;39. https://doi.org/10.15252/embj.2019103838.
78. Wei J, Nagy TA, Vilgelm A, Zaika E, Ogden SR, Romerogallo J, Piazuelo MB, Correa P, Washington MK, Elrifai W, et al. Regulation of p53 tumor suppressor by helicobacter pylori in gastric epithelial cells. Gastroenterology. 2010;139. https://doi.org/10.1053/j.gastro.2010.06.018.
79. Bhardwaj V, Noto JM, Wei J, Andl C, El-Rifai W, Peek RM and Zaika AI. Helicobacter pylori bacteria alter the p53 stress response via Erk-HDM2 pathway. Oncotarget. 2015;6. https://doi.org/10.18632/oncotarget.2828.
80. Buti L, Spooner E, Van Der Veen AG, Rappuoli R, Covacci A and Ploegh HL. Helicobacter pylori cytotoxin-associated gene A (CagA) subverts the apoptosis-stimulating protein of p53 (ASPP2) tumor suppressor pathway of the host. Proc Natl Acad Sci U S A. 2011;108. https://doi.org/10.1073/pnas.1106200108.
81. Bauer B, Moese S, Bartfeld S, Meyer TF and Selbach M. Analysis of cell type-specific responses mediated by the type IV secretion system of Helicobacter pylori. Infect Immun. 2005;*73*. https://doi.org/10.1128/IAI.73.8.4643-4652.2005.
82. Plummer M, Franceschi S, Er^ Ome Vignat J, Forman D, De Martel C. Global burden of gastric cancer attributable to Helicobacter pylori Helicobacter pylori in gastric cancer. Int J Cancer. 2015;136(2):487–90.

Publisher's Note